Extracting Simultaneous and Proportional Neural Control Information for Multiple-DOF Prostheses From the Surface Electromyographic Signal

Ning Jiang*, *Student Member, IEEE*, Kevin B. Englehart, *Senior Member, IEEE*, and Philip A. Parker, *Senior Member, IEEE*

***Abstract*—A novel signal processing algorithm for the surface electromyogram (EMG) is proposed to extract simultaneous and proportional control information for multiple DOFs. The algorithm is based on a generative model for the surface EMG. The model assumes that synergistic muscles share spinal neural drives, which correspond to the intended activations of different DOFs of natural movements and are embedded within the surface EMG. A DOF-wise nonnegative matrix factorization (NMF) is developed to estimate neural control information from the multichannel surface EMG. It is shown, both by simulation and experimental studies, that the proposed algorithm is able to extract the multidimensional control information simultaneously. A direct application of the proposed method would be providing simultaneous and proportional control of multifunction myoelectric prostheses.**

***Index Terms*—Electromyography (EMG), myoelectric control, nonnegative matrix factorization (NMF), powered prosthetics.**

I. Introduction

THE electromyographic (EMG) signal recorded at the surface of the skin contains important information regarding the state of the neuromuscular system. In particular, neural control information from higher levels of the neuromuscular system, such as the motor cortex and the spinal cord, is embedded in the surface EMG. Hence, the surface EMG has been used as a control source for powered prostheses for decades. Currently, state-of-the-art prostheses employ pattern recognition techniques to extract the neuromuscular control information from the surface EMG. Excellent performance has been achieved in terms of classification accuracy [1]–[4]; however, there are some limitations in this approach. First of all, the natural movements of limbs are continuous, but only a limited number of patterns are possible for a classifier, i.e., only a discrete approximation of the continuous parameter space of natural movements can be obtained. Increasing the number of patterns could improve the approximation, but it usually leads to more complex classifiers, more complicated and longer training processes, and deterioration of classification accuracy. Another limitation is that only one pattern or class can be designated in one decision, making pattern recognition essentially a sequential control scheme. In contrast, natural limb movements are simultaneous activations of multiple DOFs. Additionally, the pattern recognition framework does not utilize the knowledge of the underlying neurophysiological processes of natural movements gained in the past decades, such as muscle synergy and motor unit (MU) common drive. These insights are invaluable for the development of a more natural prosthesis. In a recent conference paper, we introduced a generative model of surface EMG that incorporates these neurophysiological insights [5]. In the current paper, we present a more detailed treatment of this model. Through this model, the surface EMG can be explicitly expressed as a function of multidimensional neural control information embedded within. Based on this model, we present a DOF-wise nonnegative matrix factorization (NMF) algorithm to extract the neural control information from the surface EMG, thus providing simultaneous and proportional control signals for multiple DOFs. Both simulation and experimental studies show promising results.

Manuscript received May 26, 2008; revised September 13, 2008. First published October 31, 2008; current version published May 6, 2009. This work was supported by the National Sciences and Engineering Research Council of Canada (NSERC) under Discovery Grant 217354-05 and Grant 4445-04 and by an NSERC PGS-D scholarship. *Asterisk indicates corresponding author.*

*N. Jiang was with the Department of Electrical and Computer Engineering, and the Institute of Biomedical Engineering, University of New Brunswick, Fredericton, NB E3B5A3, Canada. He is now with the Center for Sensory-Motor Interaction, Aalborg University, Aalborg, Denmark (e-mail: jiangning@hst.aau.dk).

K. B. Englehart and P. A. Parker are with the Department of Electrical and Computer Engineering, and the Institute of Biomedical Engineering, University of New Brunswick, Fredericton, NB E3B5A3, Canada (e-mail: kengleha@unb.ca; pap@unb.ca).

Color versions of one or more of the figures in this paper are available online at http://ieeexplore.org.

Digital Object Identifier 10.1109/TBME.2008.2007967

II. Methods

A. Generative Model of Surface EMG

1) Neurophysiological Processes Underlying EMG: Even the simplest natural movements of humans, such as reaching or walking, are control tasks that involve a large number of parameters, requiring precise articulations of multiple muscles and elegant coordination across multiple DOFs of multiple joints. These are daunting tasks even for the state-of-the-art robotics engineering, yet humans can perform them effortlessly. In the past decades, considerable understanding of the neuromuscular system has been gained in the field of neurophysiology. At a macroscopic level, it is has long been argued that in order to reduce the number of parameters to be controlled, the central nervous system (CNS) does not directly control each muscle. Instead, it controls a parameter set with a much smaller dimension. Over the years, different models, such as reflexes [6], unit burst generators [7], spinal force fields [8], and muscle synergy [9], [10], have been proposed to explain this dimensional reduction. A series of studies on microstimulation of interneurons in the spinal cord revealed that the force fields induced by

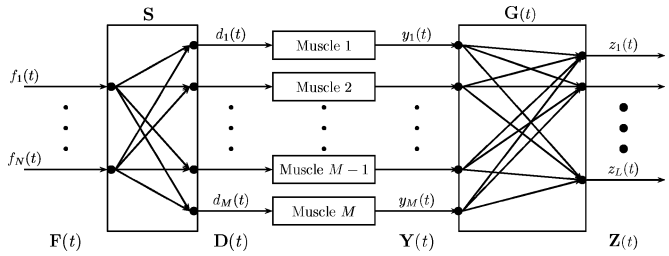

Fig. 1. Schematic diagram of the proposed generative model for surface EMG.

simultaneous stimulation of different loci of the spinal cord are linear combinations of those induced by separate stimulation of the individual locus [11]–[15]. This interesting phenomenon leads to the concept of muscle synergy, which has gained considerable attention in recent years. Strong evidence for muscle synergy has been accumulated from EMG of frogs [10], cats [16], primates [17], and humans [18], by linear decomposition algorithms such as NMF. Synergy, as defined in these studies, states that a group of muscles is activated in coordination to perform a certain task, which allows the CNS to achieve motor control tasks by controlling a small number of synergies, instead of controlling individual muscles. The existence of muscle synergy indicates that the motoneuron pools of different muscles share common neural drives. This concept of a common efferent neural drive to motoneuron pools is supported by another array of studies at a microscopic level of the neuromuscular system. In a series of studies on the firing patterns of MUs, the smallest functional unit of muscular system, DeLuca *et al.* showed that MUs within a muscle change their firing rates in concert, indicating that they share a common neural drive. This phenomenon is called "common drive" [19]. It is also shown that common drive exists among MUs from synergistic muscle pairs [20] and antagonist muscle pairs during coactivation [21]. There is evidence that common drive arises from the spinal level [22], as do the neural structures encoding muscle synergy [9].

2) Generative Model of Surface EMG: Based on the neurophysiology discussed before, we propose a generative model for surface EMG. A schematic diagram of this model is shown in Fig. 1. The model assumes that there exists control information at the spinal level. In the context of the myoelectric control, the model further quantifies the control information as a set of time-varying *force functions*, with a dimension equal to the number of DOFs of the limb movement. The *force functions* represent the intended activation levels of all the DOFs. Without loss of generality, consider a simple case where a movement involves only one joint, which has N DOF. Define the *force functions* of this joint as $\mathbf{F}(t)$

$$\mathbf{F}(t) = [f_1(t), f_2(t), \ldots, f_N(t)]^T \tag{1}$$

where $f_n(t)$ is the *force function* of the nth DOF. The maximum frequency of the *force functions* is f_f, which is limited by the physiological ability of neuromuscular system, arguably lower than 5 Hz [23]. Next, assuming that M muscles are involved in the movements of this joint, the activation function vector of all these muscles is $\mathbf{X}(t)$

$$\mathbf{X}(t) = [x_1(t), x_2(t), \ldots, x_M(t)]^T \tag{2}$$

where $x_m(t)$ is the activation function of the mth muscle, which is the neural drive directly applied to this muscle. The activation vector is an instantaneous mixture of $\mathbf{F}(t)$

$$\mathbf{X}(t) = \mathbf{S} \cdot \mathbf{F}(t) \tag{3}$$

where $\mathbf{S} = \{s_{mn}\}$ is an $M \times N$ matrix and s_{mn} indicates the extent to which the mth muscle is participating in the activation of the nth DOF. The instantaneous mixing process in (3) generates synergies among the muscles at this joint. Note that $\mathbf{X}(t)$ has the same bandwidth as $\mathbf{F}(t)$. If an intramuscular electrode is placed close to each of the muscles to detect their activities, assuming no significant crosstalk between the electrodes, the EMG of the mth muscle, namely $y_m(t)$, is

$$y_m(t) = \sum_{j=1}^{N_m} g_{mj}(t) * f_{mj}[x_m(t)] \tag{4}$$

where N_m is the number of MUs in the mth muscle, $g_{mj}(t)$ is the volume conductor between the electrode and the jth MU of the muscle, and $*$ is a convolution operator. The symbol $f_{mj}[\bullet]$ is the firing sequence of the jth MU of the muscle. It incorporates two force modulation strategies: integral pulse frequency modulation (IPFM) property of the MU (rate coding) and the ordered recruitment of the MU pool. Equation (4) is a very complex nonlinear transformation. In a recent study on the spectrum of modulated EMG, the authors have shown that the mean square value (MSV), obtained by a square operator followed by a low-pass filter, can be used as the demodulator of $y_m(t)$ to extract the modulation signal $x_m(t)$ [24]. From this result and denoting the MSV of $y_m(t)$ by $\widehat{y_m^2(t)}$, it follows that

$$\widehat{y_m^2(t)} = \frac{1}{T}\int_t^{t+T} y_m^2(\tau)d\tau \simeq h_m \cdot x_m(t) \tag{5}$$

where h_m is a constant that depends on both $g_{mj}(t)$ and $f_{mj}[\bullet]$, and T is the width of the average time window. The low-pass filtering operation by which the MSV is obtained should have a cutoff frequency f_F equal to or larger than the bandwidth of $\mathbf{F}(t)$. Considering all muscles involved, (5) can be further written in a matrix form

$$\widehat{\mathbf{Y}^2(t)} = \mathbf{H} \cdot \mathbf{X}(t) \tag{6}$$

where $\widehat{\mathbf{Y}^2(t)}$ is

$$\widehat{\mathbf{Y}^2(t)} = \left[\widehat{y_1^2(t)}, \widehat{y_1^2(t)}, \ldots, \widehat{y_M^2(t)}\right] \tag{7}$$

and $\mathbf{H}$ is a diagonal matrix with

$$\mathbf{H} = \text{diag}[h_1, h_2, \ldots, h_M]. \tag{8}$$

Combining (3) and (6), it follows that

$$\widehat{\mathbf{Y}^2(t)} = \mathbf{H} \cdot \mathbf{S} \cdot \mathbf{F}(t). \tag{9}$$

The solution of (9) is a rather simple instantaneous linear mixture problem. By implicitly assuming (9), various linear decomposition algorithms have been applied to solve the

mixture using $\widehat{\mathbf{Y}^2(t)}$ (see a review by Tresch *et al.* [25]). These studies employed either indwelling electrodes (for animal studies) or distantly separated surface electrodes (for human studies) [18], where crosstalk is negligible [26]. This, however, is not the case for most surface EMG recordings, where crosstalk between channels is significant [27]–[29]. Consequently, from Fig. 1, the observed L-channel surface EMG, namely $\mathbf{Z}(t) = [z_1(t), z_2(t), \ldots, z_L(t)]$, is

$$z_l(t) = \sum_{m=1}^{M} z_{lm}(t) = \sum_{m=1}^{M} \sum_{j=1}^{N_m} g_{mj}^{l}(t) * f_{mj}[x_m(t)] \quad (10)$$

where $z_{lm}(t)$ is the contribution from the mth muscle to the overall surface EMG detected by the lth electrode and $g_{mj}^{l}(t)$ is the volume conductor filter between the jth MU of the mth muscle and the lth surface electrode. Evidently, $z_l(t)$ is not an instantaneous mixture, but a convolutive one. Recently, Farina *et al.* have attempted to solve the mixture using blind source separation (BSS) algorithms [30], [31]. Two fundamental assumptions of these studies are uncorrelated $x_m(t)$ and instantaneous mixtures, both of which would be seriously challenged for multichannel nonstationary surface EMG due to crosstalk and a volume conductor filter. In the present study, an alternative approach is proposed to extract or estimate the *force functions* from the surface EMG. Using the same demodulator as in (5), the MSV of $z_{lm}(t)$ can be written as

$$\widehat{z_{lm}^2(t)} = h'_{lm} \cdot x_m(t) \quad (11)$$

where h'_{lm} is a constant dependent on $g_{mj}^{l}(t)$ and $f_{mj}[\bullet]$. Now, the MSV of $z_l(t)$ is

$$\widehat{z_l^2(t)} = \sum_{m=1}^{M} \widehat{z_{lm}^2(t)} + \sum_{m=1}^{M} \sum_{\substack{k=1 \\ k \neq m}}^{M} \widehat{z_{lm}(t) \cdot z_{lk}(t)}. \quad (12)$$

From (12), it is clear that $\widehat{z_l^2(t)}$ is an instantaneous nonlinear mixture of the *force functions* and $\widehat{\mathbf{Z}^2(t)}$ is the multidimensional instantaneous nonlinear mixture of the *force functions*

$$\widehat{\mathbf{Z}^2(t)} = \mathbb{T}[\mathbf{F}(t)] \quad (13)$$

where $\mathbb{T}[\bullet]$ is an unknown complex nonlinear transformation. Usually in myoelectric control, only $\mathbf{Z}(t)$ is readily available, and estimating the latent $\mathbf{F}(t)$ in (13) becomes an instantaneous nonlinear BSS problem. Such problem, in general, has no solutions [32]. However, the nonlinearity in (13) diminishes when the following two conditions are satisfied.

1) Crosstalk between surface EMG channels is small, or $x_m(t)$ and $x_k(t)$ have low correlation, such that the cross-product terms in (12) are negligible.
2) The MSV of the EMG from a muscle is approximately linear with respect to its activation function, i.e., the approximation in (5) holds, in spite of the nonlinearity caused by the two force modulation strategies.

These two conditions hold reasonably well in practice. Thus, they will be assumed in the first solution attempt, and (13) reduces to a linear mixture

$$\begin{aligned} \widehat{\mathbf{Z}^2(t)} &= \mathbf{H}' \cdot \mathbf{S} \cdot \mathbf{F}(t) \\ &= \mathbf{W} \cdot \mathbf{F}(t) \end{aligned} \quad (14)$$

where $\mathbf{H}' = \{h'_{lm}\}$ is an $L \times M$ matrix and $\mathbf{W}$ is an $L \times N$ matrix. Now, extracting $\mathbf{F}(t)$ from $\widehat{\mathbf{Z}^2(t)}$ becomes an instantaneous linear BSS problem, and a semi-unsupervised source separation algorithm is proposed next to estimate $\mathbf{F}(t)$ in (14). The factors affecting the linear approximation and the estimation performance of the linear algorithm will be examined through simulation and experimental studies.

3) DOF-Wise NMF Algorithm: The NMF algorithm is a multivariate statistical data analysis technique. For a linear mixture such as (14), where only $\widehat{\mathbf{Z}^2(t)}$ is available, and both $\mathbf{W}$ and $\mathbf{F}(t)$ are latent, it seeks to find an approximate solution to the equation only with the restriction that all elements in the equation are nonnegative. It has been successfully applied in extracting muscle synergies from multichannel EMG in many studies (for a review of these studies, refer to [25]). However, in these studies, the physiological relevance of the extracted synergy is not clear, largely due to the fact that the solutions obtained by NMF are not unique, both in the order of the synergies and their respective amplitudes. This indeterminacy is a serious issue for myoelectric control, where physiological relevance is essential: one must have the knowledge regarding which DOF is active and how much it is active in order to provide meaningful control information. As such, extra information regarding the *force functions* must be incorporated to minimize the indeterminacy. The semi-unsupervised approach is preferred since it is more appealing than the previously proposed supervised approach [5]. This is particularly true for clinical applications, where the target, i.e., *force functions*, are usually not available.

In order to apply NMF algorithm in the context of myoelectric control, i.e., satisfying the nonnegative requirement of NMF, define $f_i^+(t)$ and $f_i^-(t)$ as

$$\begin{aligned} f_i^+(t) &= f_i(t), \quad \text{when } f_i(t) \geq 0 \\ f_i^-(t) &= -f_i(t), \text{ when } f_i(t) < 0 \end{aligned} \quad (15)$$

where $f_i(t)$ is the ith *force function* defined in (1). Now $\mathbf{F}(t)$ can be rewritten as

$$\mathbf{F}(t) = [f_1^+(t), f_1^-(t), f_2^+(t), f_2^-(t), \ldots, f_N^+(t), f_N^-(t)]^T \quad (16)$$

and (14) can be rearranged into a DOF by DOF form

$$\widehat{\mathbf{Z}^2(t)} = [\, W_1^+ \quad W_1^- \quad \cdots \quad W_N^+ \quad W_N^- \,] \cdot \begin{bmatrix} f_1^+(t) \\ f_1^-(t) \\ \cdots \\ \cdots \\ \cdots \\ f_N^+(t) \\ f_N^-(t) \end{bmatrix}. \quad (17)$$

Now, when the only nonzero member functions of $\mathbf{F}(t)$ are $f_i^+(t)$ and $f_i^-(t)$ corresponding to the scenario when only the

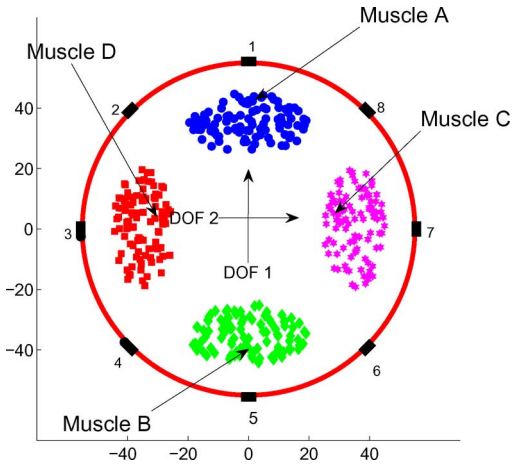

Fig. 2. Geometry of the simulated muscle, DOF, and electrodes. Units of both axes are in millimeters.

ith DOF is activated, (17) reduces to

$$\widehat{\mathbf{Z}_i^2(t)} = [\, W_i^+ \quad W_i^- \,] \cdot \begin{bmatrix} f_i^+(t) \\ f_i^-(t) \end{bmatrix} \tag{18}$$

where $\widehat{\mathbf{Z}_i^2(t)}$ is the MSVs of the $\widehat{\mathbf{Z}^2(t)}$ when only the ith DOF is activated. This "divide and conquer" approach divides the task of solving the mixture in (14) to the task of solving N simpler mixtures such as the one in (18), each of which can be solved by a standard NMF algorithm. The only indeterminacy of the solution with this approach is the order within each subproblem, i.e., the sign of the obtained *force function* of each DOF, which is trivial to solve by proper data collection protocol design. The NMF algorithm implemented in this study utilizes the least mean square cost function and the multiplicative minimization routine, as presented in [33].

B. Simulation Studies

1) EMG Simulation: A MATLAB simulation of the EMG generation process was implemented based on the generative model proposed. Two DOFs, four muscles (two agonist/antagonist pairs), and eight bipolar surface electrodes were simulated. The geometric configuration of the simulation is shown in Fig. 2. A circular limb cross section of radius 55 mm is assumed with the four muscles located as shown in the figure. An electrode array of eight bipolar electrodes were equally spaced around the circumference of the limb. Each of the four muscles is the prime mover of one DOF and the secondary mover of another DOF, i.e., a co-contraction muscle with the prime mover, at a lower contraction level. Muscles A and B are the prime flexor and extensor of DOF 1, and the secondary flexor and extensor of DOF 2, respectively; C and D are the prime flexor and extensor of DOF 2, and the secondary flexor and extensor of DOF 1, respectively. A positive value of a *force function* excites the flexors and inhibits the extensors at the corresponding DOF. Conversely, a negative value has the opposite effects on the muscles. To reflect the fact that the prime mover contributes more forces than the secondary mover, without loss of generalization, the activation coefficients in (3) for the prime mover and the secondary mover at a DOF are 0.7 and 0.3, respectively. Therefore, the mixing matrix $\mathbf{S}$ is

$$\mathbf{S} = \begin{bmatrix} 0.7 & -0.7 & 0.3 & -0.3 \\ 0.3 & -0.3 & 0.7 & -0.7 \end{bmatrix}^T. \tag{19}$$

The activation function vector $\mathbf{X}(t)$ was obtained by multiplying the *force functions* $\mathbf{F}(t)$ and the mixing matrix $\mathbf{S}$. Each muscle had a pool of 100 MUs. The innervation processes, i.e., the firing times of the MUs, were simulated using an IPFM model [34], and the ordered recruitment of the MUs was implemented using the exponential threshold method described in [35]. The minimum and maximum average firing rates of all the MUs were 8 and 40 Hz, respectively. The average coefficient of variation of the interpulse intervals (IPIs) of all MUs is 15%. The MU action potentials (MUAPs) were generated using a volume conductor model [36], and the MUAP trains were generated by convolving the MUAPs with their corresponding innervation processes. The summation of all MUAP trains from all muscles detected at a recording electrode generated the corresponding surface EMG, as described in (10). Twenty simulation sessions were generated, each consisting of five sections, corresponding to five types of $\mathbf{F}(t)$, as shown in Fig. 6. The first type was designed such that only one DOF was activated at a time, and it was designated as the training dataset. For the other four sections (slow Gaussian profile, slow random profile, fast Gaussian profile, and fast random profile), the two DOFs were simultaneously activated, and they were designated as the testing datasets. The Gaussian profiles were similar to those implemented in [30]. The random profiles were designed to demonstrate the ability of the proposed method to learn the mixture, rather than the temporal characteristic of the *force functions*.

To analyze the effect of nonlinearity, particularly the nonlinearity due to nonzero cross-product terms in (12), the contribution from each muscle to the eight electrodes were manually scaled to produce different levels of crosstalk. This manual scaling process is illustrated in Fig. 3 for muscle A. The signal contributions of the other three muscles were scaled similarly.

2) Data Processing: The MSVs of the simulated EMG (original and manually scaled) were obtained by a 200-ms rectangular smoothing window. For each simulation session at each scaling level, two estimations for the *force functions* were obtained using the proposed DOF-wise NMF algorithm. For the first estimation, all eight channels of MSVs were used. For the second estimation, only a four-channel subset of the MSVs was used. The four selected channels are 1, 3, 5, and 7, which are located directly above the four muscles and have the least amount of crosstalk. In either case, the estimates of W_i^+ and W_i^- in (18) were obtained DOF by DOF from the MSVs of the training datasets. Once the mixing matrix was estimated, the MSVs from the testing datasets were used to calculate the corresponding *force function* estimations, directly from (14). The performance of each estimation was quantified using the index presented in Section II-D.

One of the desirable features of the proposed algorithm is that it is semi-unsupervised, in a sense that the only information regarding the *force functions* required during training is which

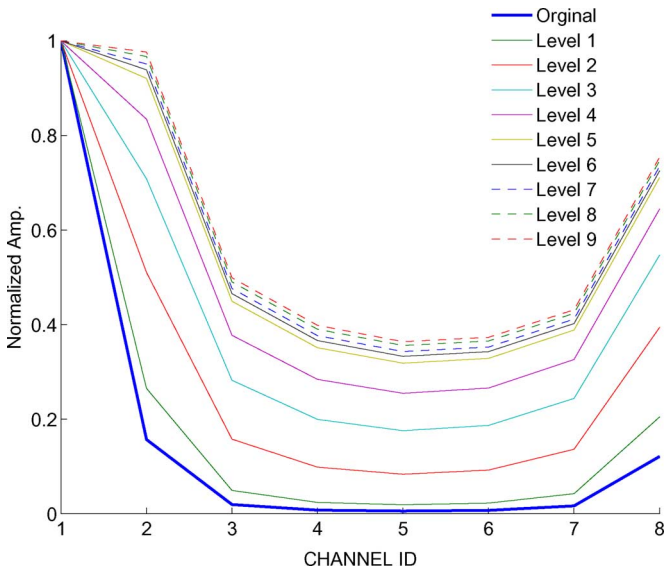

Fig. 3. Different levels of simulated crosstalk. The magnitude of crosstalk is generated by muscle A, and the values are normalized with respect to the magnitude of channel 1 (refer to Fig. 2). The crosstalk level before the manual scaling is indicated by the thick blue line. The other nine crosstalk levels are plotted as thin lines.

DOF is activated. To further demonstrate the power of this characteristic of the algorithm, a comparison of its performance and that of a direct approach is made. The direct approach estimates the mixing matrix directly from (14), using the MSVs and the corresponding *force functions* of the training dataset. The estimates of the *force functions* of the testing datasets were calculated the same way as in the DOF-wise NMF algorithm.

The proposed algorithm is a linear method. Its performance is based on the linear assumptions discussed in Section II-A2. To show the effect of nonlinearity in the system, the *force functions* were also estimated by a nonlinear artificial neural network. A multilayer perceptron network (MLP) with one hidden layer was created. The transfer function of the neurons in the hidden layer and the output layer are "*tan-sigmoid*" and "*linear*," respectively. The inputs and the targets of the MLP are the MSVs of the simulated EMG and *force functions*. The network was trained using the training datasets and tested on the testing datasets.

C. Experiment Studies

1) General Protocol: The experiment protocol of this study was approved by the Research Ethics Committee of the University of New Brunswick (REB File #: 2007-095). A total number of 12 subjects with no known neuromuscular disorders (seven males and five females, aged from 25 to 50 years) participated in the experiment. The wrist was selected as the joint of interest, as there is a great demand for a more usable and functional wrist in transradial prostheses. Also, the wrist is a simpler joint compared with the shoulder joint, yet it is complex enough to have three DOFs: wrist flexion/extension, radial/ulnar deviation, and wrist pronation/supination. During an experiment session, the subject sat in a chair with an armrest on which the right upper arm and forearm of the subject were secured. The right hand of the subject was fixed at a neutral, palm facing inward, position by a custom-made handle. The handle was attached to a heavy duty steel frame. A six-axial force/torque transducer was mounted between the handle and the steel frame. Eight surface electrodes were placed on the arm collect surface EMG: seven equally spaced around the forearm and one on the bicep. The subject was then instructed to perform a series of dynamic wrist contractions, at low to medium force levels, during which both forces at the three DOFs and the surface EMG were acquired. The details of these wrist contractions and the data collection procedure are discussed in subsequent sections. The experiment setup is shown in Fig. 4.

2) Wrist Contractions: There are three DOFs at the wrist: flexion/extension (DOF 1), radial/ulnar deviation (DOF 2), and pronation/supination (DOF 3). More complex wrist movements are combined activations of these three DOFs. During a data collection session, the forces produced by the wrists of the subjects at the three DOFs were detected by a six-axial force/torque transducer (Gamma FT-130-10, ATI Industries). The analog force signals were sampled at 1 kHz and digitized by a digital data acquisition card (DAS1602 DAQ card, Measurement Computing). To help the subjects produce the desired contractions, a 3-D pyramid visualizing the forces produced was displayed to the subjects in real time. The apex of the pyramid was fixed in the 3-D space, pointing away from the subjects, with its base facing the subject, moving in accordance with the forces produced by the subjects. Forces on DOF 1 would produce horizontal tilting of the pyramid (left/right); forces on DOF 2 would produce vertical tilting (up/down); forces on DOF 3 would produce rotation of the base around the axis running through the center of the base and the apex of the pyramid. The pyramid shown in Fig. 4 indicates that the subject is producing flexion, ulnar deviation, and pronation simultaneously. In the beginning of an experiment session, the subject would first familiarize him or herself with the force transducer through the 3-D visual feedback. The subject was then instructed to perform a series of predefined contractions. An entire data collection is composed of seven sets, each containing several contractions. Among these seven sets, sets 1, 2, and 4 were training sets, since only one DOF was intended to be activated at a time. The other four sets, 3, 5, 6, and 7, were testing sets since multiple DOFs were intended to be activated simultaneously. The details of these contractions are summarized in Table I. Each contraction in sets 5, 6, and 7 were 15 s in duration, and contractions in the other four sets were 30 s in duration. The subjects took rest periods between contractions to avoid fatigue. The length of the resting period was under the discretion of the subjects. Since the contractions are not long, and not at high contraction levels, no subject reported fatigue during or at the end of the experimental sessions. A complete experiment session lasted from 1.5 to 2 h.

3) EMG Collection and Processing: The EMG of the wrist muscles and *biceps brachii* were detected using the eight DuoTrode bipolar surface electrodes, sampled at 1 kHz, digitized by a second data acquisition card (PCI6024E, National Instrument), and synchronized with the force signals. The EMG signals were displayed on the monitor in real time to ensure quality.

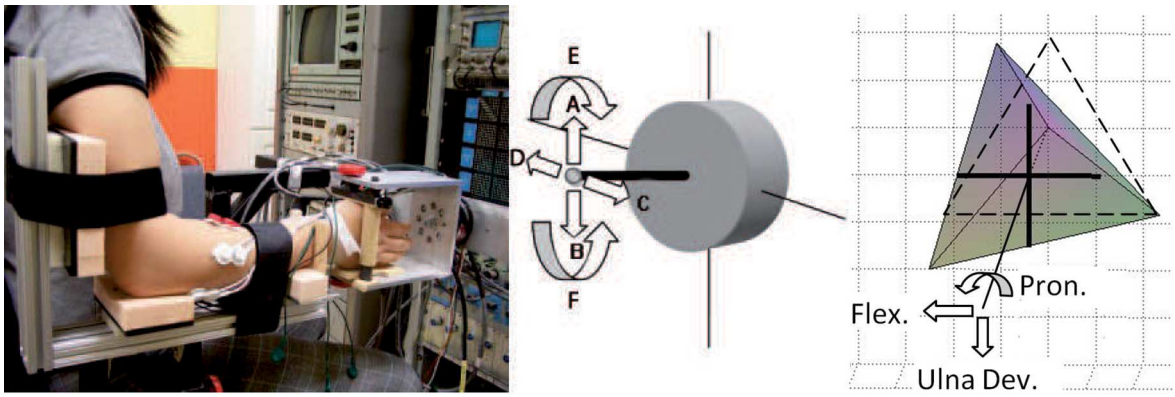

(a) (b)

Fig. 4. (a) Experiment setup. The force transducer (enlarged illustration on the right) is located between the handle securing the palm and the steel frame. The sensed DOFs are: A/B→ flexion/extension, C/D → radial/ulnar deviation, E/F→ pronation/supination. (b) 3-D visualization of the forces produced by wrist. The broken triangle indicates the resting position of the face of pyramid. The displacement of the pyramid in the figure is due to simultaneous activations of flexion, ulnar deviation, and pronation.

TABLE I
DETAILS OF EXPERIMENT PROTOCOL

SECTION	DESCRIPTION	CONTRACTIONS
1. DOF 1	Sinusoidal contraction, alternating between flexion and extension	2 contractions: move the pyramid left and right
2. DOF 2	Sinusoidal contraction, alternating between radial and ulnar deviation	2 contractions: move the pyramid up and down
3. Combination 1&2	Combined activation of DOF 1 and DOF 2	**1**: move the pyramid in a clockwise circle **2**: move the pyramid in a counterclockwise circle **3**: move the pyramid on the forward diagonal line **4**: move the pyramid on the backward diagonal line
4. DOF 3	Sinusoidal contraction, alternating between supination and pronation	2 trials: rotating the pyramid clock wise (sup.) and counter clockwise (pro.)
5. Combination 1&3	Combined activation of DOF 1 and DOF 3	**1**: move the pyramid left and right (flex./ext.), while keep a clockwise rotation (pro.) **2**: move the pyramid left and right (flex./ext.), while keep a counter clockwise rotation (sup.) **3**: keep the pyramid to the left hand side (flex.), while rotating the pyramid in both directions (sup./pro.) **4**: keep the pyramid to the right hand side (ext.), while rotating the pyramid in both directions (sup./pro)
6. Combination 2&3	Combined activation of DOF 2 and DOF 3	**1**: move the pyramid up and down (radial/ulnar dev.), while keep a clockwise rotation (pro.) **2**: move the pyramid left and right (radial/ulnar dev.), while keep a counter clockwise rotation (sup.) **3**: keep the pyramid to the upper side (radial dev.), while rotating the pyramid in both directions (sup./pro.) **4**: keep the pyramid to the lower side (ulnar dev.), while rotating the pyramid in both directions (sup./pro)
7. Combination 1&2&3	Combined activation of all three DOFs	**1**: move the pyramid in a clock wise circle (combo 1&2), while keep a clockwise rotation (pro.) **2**: move the pyramid a counter clock wise circle (combo 1&2), while keep a counter clockwise rotation (sup.) **3**: keep the pyramid to the upper left corner (flex.& radial dev.), while rotating the pyramid in both directions (sup./pro.) **4**: keep the pyramid to the lower left side (fle. & ulnar dev.), while rotating the pyramid in both directions (sup./pro)

The EMG acquired in experiment studies were processed in the same way as the simulated EMGs. For each subject, the mixing matrix was estimated by the DOF-wise NMF algorithm using the MSVs from the training datasets (sets 1, 2, and 4). The estimated mixing matrix was then used in (14) to estimate the forces produced during the testing sets (3, 5, 6, and 7).

The forces produced during the testing sets were also estimated by the direct linear matrix method and the nonlinear

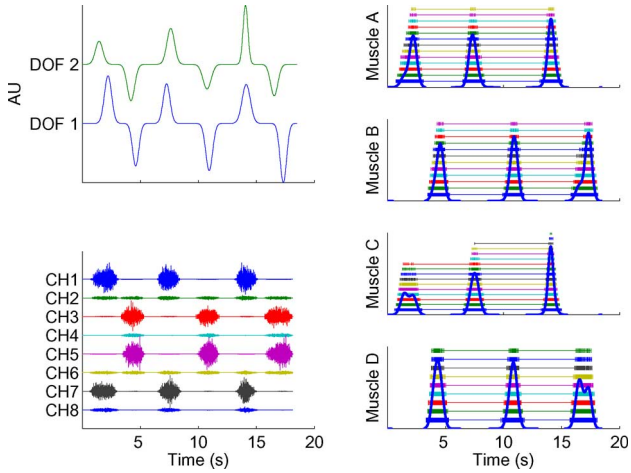

Fig. 5. Simulation data of type 2 *force function* from one simulation session. The *force functions* are plotted in the top left panel. The unit of the vertical axis is arbitrary. The activation functions for each muscle and the corresponding IPI bar plot of the MU pools are presented in the right panel. The solid line in each subplot is the activation functions for the muscle. Note that the negative phase of the activation function is not shown. Each short vertical bar represents a firing of an MU. The MUs are arranged by their recruitment thresholds. The resulting eight-channel EMGs are plotted in the bottom left panel.

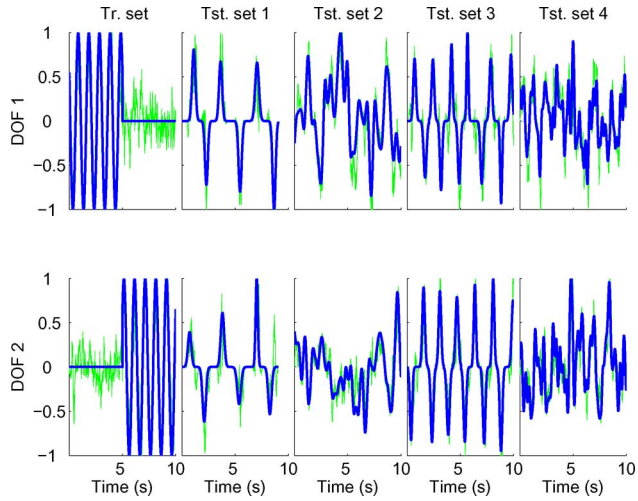

Fig. 6. Estimation results of one simulation session with the most significant crosstalk (level 9). The upper row is DOF 1 and the lower row is DOF 2. The leftmost column is the training dataset where only one DOF is activated at a time. The other four columns are the testing dataset. From left to right: slow Gaussian profile, slow random profile, fast Gaussian profile, and fast random profile. The thick line in each plot is the *force functions* and the thin line is the estimated *force functions* when the four-channel subset is used. The R^2 value is 83.3%.

MLP approach, as discussed in the data processing for simulation studies. The estimation performances of the three methods were measured by the performance index presented next.

D. Performance Measure

To quantify the performance of the proposed *force function* estimation method, multivariate R^2 indexes similar to that used in [18] were employed. The global R^2 for a simulation or an experiment session is defined as

$$R^2 = 1 - \frac{\sum_{i=1}^{D}\sum_{t=0}^{N}\left(\widehat{f_i(t)} - f_i(t)\right)^2}{\sum_{i=1}^{D}\sum_{t=0}^{N}\left(f_i(t) - \overline{f_i(t)}\right)^2} \qquad (20)$$

where D is the number of *force functions*, N is the number of data points, $f_i(t)$ is the ith *force function*, $\widehat{f_i(t)}$ is the corresponding estimate, and $\overline{f_i(t)}$ is the temporal average of $f_i(t)$. The numerator is the total mse of the estimates and the denominator is the total variance of the *force functions*. Equation (20) provides a good global measure of the estimation performance for a simulation or an experiment session. It provides the percentage of total variation in the *force functions* captured by the estimates. The larger the value, the better the estimation performance. The index assumes its upper bound of unity in the case of perfect estimate (zero mse).

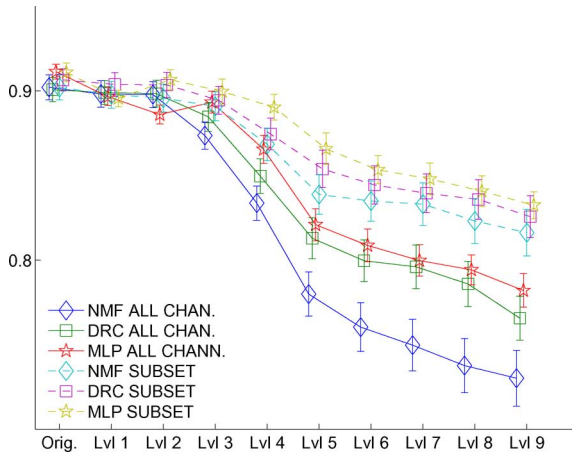

Fig. 7. Comparison of the estimation performances of the three methods for simulation data. Each data point is the mean R^2 values over the 20 simulation sessions at a particular combination of crosstalk level, MSVs used, and estimation method. The vertical lines indicate the corresponding standard deviation. The solid lines and the dashed line are the results when all eight channels of MSVs are used and the four-channel subset are used, respectively. The diamonds, squares, and stars denote results obtained by the proposed DOF-wise NMF algorithm, the linear direct method, and the nonlinear MLP approach, respectively.

III. Results

A. Simulation Results

The *force functions*, firing times of the MU pools of the four muscles, and the simulated eight-channel EMG of one section (type 2) from one simulation session are plotted in Fig. 5. The estimated *force functions* of one simulation session with the largest crosstalk (level 9) are plotted in Fig. 6. The estimation performances with different crosstalk levels, estimation methods, and number of EMG channels are plotted in Fig. 7. The R^2 value decreases when the level of crosstalk increases, both with eight channels of data and with the four-channel subset. The effect of the crosstalk is also demonstrated by the fact that with the four-channel subset, the estimation performance is always better than when all eight channels are used. This is expected since these four channels are directly located above the four muscles and have the least crosstalk.

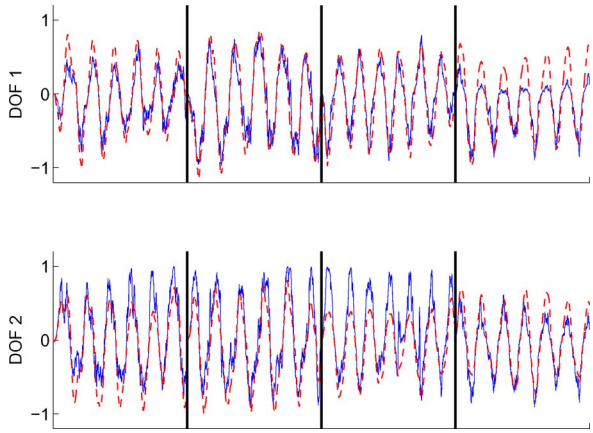

Fig. 8. Estimation results of one subject (#10) when DOF 3 is excluded (the four contractions from experiment set 3). Top row is DOF 1 (flexion/extension) and bottom row is DOF 2 (radial/ulnar deviation). The solid lines are the estimated forces and the dashed lines are the corresponding forces. The R^2 value for the data shown is 87.21%.

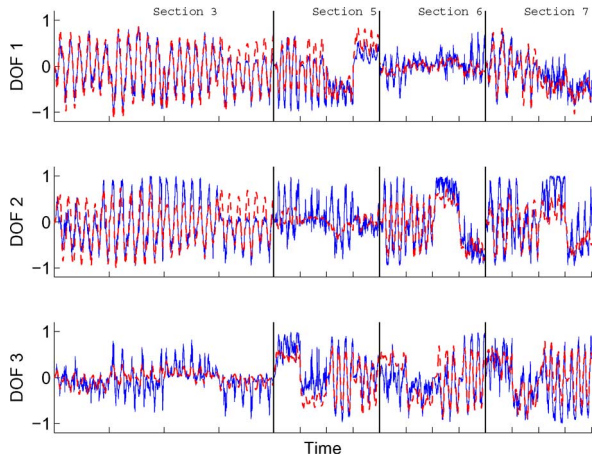

Fig. 9. Estimation results of one subject (#10) when DOF 3 is included. Datasets 3, 5, 6, and 7 are indicated by the four vertical separation lines. The ticks at the time axis indicate the contractions within each set. Top row is DOF 1, middle row is DOF 2, and the bottom row is DOF 3. The solid lines are the estimated forces and the dashed lines are the recorded forces at the corresponding DOFs. The R^2 for the data shown is 54.2%.

In general, the estimation performance of the proposed algorithm is high. In the best case, using the original data (no manual scaling), the R^2 values of the 20 sessions are $90.2 \pm 0.740\%$ when using all eight channels and $90.2 \pm 0.630\%$ when using the four-channel subset. The high performance in this case indicates that the proposed algorithm is not sensitive to the nonlinearity between the MSV and the neural drive, introduced by the force modulation strategies.

Further, for the worst case (crosstalk level 9), in addition to the nonlinearity induced by the two force modulation strategies, the nonlinearity of the second term in (12) is significant. In this case, the R^2 values over the 20 sessions are $73.0 \pm 1.65\%$ when using all eight channels and $81.6 \pm 1.37\%$ when using the four-channel subset of data. This result shows that even with high levels of crosstalk, by properly placing recording electrodes, the proposed algorithm is able to maintain a relatively high estimation performance: using the four-channel subset provides almost 10% of performance boost over using all eight channels.

The number of hidden neurons in the MLP network was chosen to be 2 since a network with more than two hidden neurons showed significant overfitting. The performance of the nonlinear MLP, the direct linear matrix method, and the proposed DOF-wise NMF algorithm are plotted in Fig. 7 for all the 20 simulation sessions. The nonlinear MLP performs best among the three and the direct linear method performs better than the proposed algorithm. However, the differences are not dramatic, and the performance of the proposed method is very encouraging considering that it is semi-unsupervised and linear.

B. Experimental Results

Of the 12 subjects, 11 were able to complete the entire experiment session. Two estimations were obtained for each of the 11 subjects, one on the data excluding DOF 3 and one on all data.

The estimation results for one subject using the proposed algorithm are shown in Figs. 8 (excluding DOF 3) and 9 (including DOF 3). The estimation performances of the proposed algorithm are presented in Fig. 10. The R^2 values for all subjects are $77.5 \pm 10.9\%$ when DOF 3 is excluded; the R^2 values are $-60.1 \pm 132\%$ when DOF 3 is included. In general, when DOF 3 is excluded, the estimation performance is close to those obtained in simulation studies. However, the estimation performance is very poor when DOF 3 is included. The estimation errors in the experimental results are due to three main factors: force translations across the DOFs, nonlinearities in system, and operator error.

1) Effects of Force Translation: Even though the design of the experiment apparatus was to ensure that the rotational axis of the wrist of the subject is aligned with the axis of the force sensor, there were force translations from one DOF to the other two DOFs, particularly when DOF 3 is activated. These force translations across the DOFs can be modeled as an additional mixing matrix in the generative model. However, it constitutes a serious problem for the DOF-wise NMF algorithm because the only inputs to the algorithm are the MSVs, and it does not have any knowledge about the force translation. In order to examine the effect of the force translation, the direct estimation method introduced in Section II was used to estimate the forces. Since the direct estimation method utilized the recorded forces during training, its performance should not be affected by the force translations. The estimation performance of the direct estimation method of all subjects is plotted in Fig. 10. For this method, the R^2 values are $78.5 \pm 7.62\%$ when DOF 3 is excluded and $31.2 \pm 17.4\%$ when DOF 3 is included. Evidently, the direct approach provides a significant performance gain over the NMF approach by utilizing the recorded forces as part of the training process. This is particularly true when DOF 3 was included in the analysis. Further analysis demonstrated that the performance gain obtained by the direct method is strongly correlated with the amount of force translations in the training set. Linear regression analyses found significant correlation between

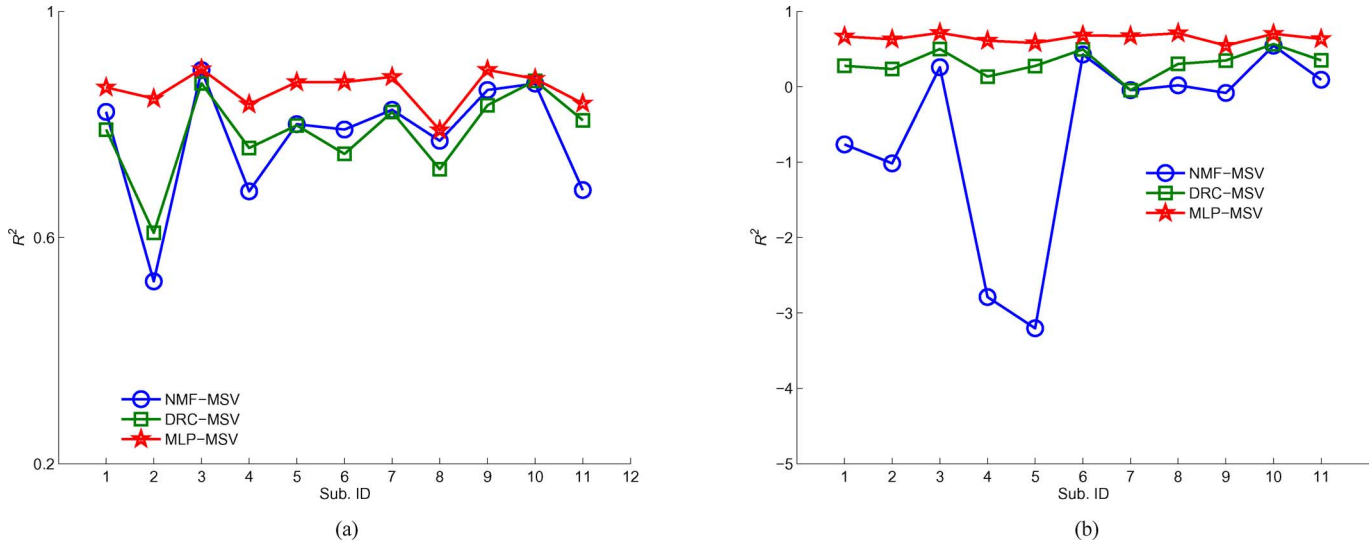

Fig. 10. Performances of the proposed DOF-wise NMF algorithm, the direct matrix method, and the nonlinear MLP algorithm. (a) DOF 3 is excluded. (b) DOF 3 is included.

the performance gain and the force translations ($r^2 = 37.8\%$, $p = 0.0371$ when DOF 3 is excluded and $r^2 = 79.7\%, p < 10^{-5}$ when DOF 3 is included). This result indicates that a better alignment of the axis of wrist and the force sensors would enhance the performance of the proposed NMF algorithm in this experiment.

2) Effects of Nonlinearities in System: As discussed in Section II, the force modulation strategies of the neuromuscular system and surface EMG crosstalk can produce nonlinearities in the generative model of surface EMG, which would affect the estimation performance of the linear DOF-wise NMF estimator. The effects of these nonlinearities are assessed by comparing the estimation performances of the proposed method and that of the nonlinear MLP estimator processing the same experimental data. The number of hidden neurons in the MLP was chosen to be 3 since significant overfitting occurred when the number was larger than 3. The performances of the MLP algorithm are also plotted in Fig. 10. When DOF 3 is excluded, the R^2 values obtained by the MLP algorithm are $86.2 \pm 3.23\%$. When DOF 3 is included, the R^2 values are $64.9 \pm 5.49\%$. The dramatic enhancement in the estimation performance when DOF 3 is included can be explained by the fact that the crosstalk is much more significant in this case, because more muscles located closely are activated. Consequently, the cross-product terms in (12) become more significant. The nonlinear MLP algorithm is able to capture the nonlinearity of the system, while two linear approaches are not.

3) Inadvertent Subject Alignment and Position Changes: The third source error is noted by the large variability across subjects in the estimation performances (refer to Fig. 10) even when the nonlinear MLP estimator was used. Some subjects found it intuitive to perform the required contractions, while some found it very unnatural and difficult with wrist restricted, particularly for supination/pronation (DOF 3). Also, it was noticed that some subjects tended to move their upper arm or trunk to help produce the desired forces. This means that the forces recorded by the sensor were not just produced by the forearm muscles. As a result, the estimation would have significant undershoot, since the estimation algorithms had the knowledge regarding only the contractions of the forearm muscles. In Fig. 8, this type of undershoot is particularly significant for the last contraction, possibly due to fatigue in the forearm muscles resulting in the recruitment of other muscles.

IV. Discussion and Conclusion

A. Errors Analysis

The experiment results are encouraging as they showed that the proposed DOF-wise NMF algorithm has the capability to estimate the forces produced at multiple DOFs during dynamic contractions by using only the MSVs of the multichannel surface EMG. The performances of the algorithm were close to those obtained in the simulation study when DOF 3 is excluded. When DOF 3 is included in the analysis, the performance degraded dramatically, due to the surface crosstalk and the increased amount of force translations (an experimental design issue).

In the clinical context, surface crosstalk can be a challenging issue. More selective surface electrodes and better placement of the electrodes can help to reduce crosstalk. Proper signal preprocessing to the raw EMG signals can also reduce crosstalk. It should be noted that the proposed method is much less sensitive to crosstalk than the traditional one-site/one-function prosthesis control approach since its performances on the first two DOFs are quit impressive, while the traditional approach would fail due to crosstalk.

The force translation affects the estimation performance reported in this study since the recorded forces are used as the targets. This is not an issue in clinical setting since force signals are not available in the first place. And the ability of the proposed algorithm to estimate forces, or intended activations,

in a semi-unsupervised fashion (without actually recording the forces) is one of its most appealing characteristics. To measure the performances of the proposed algorithm in a clinical setting, it is possible to use some virtual targets or some other objective goals.

B. Conclusion

This study proposed a DOF-wise NMF algorithm to extract neural control information from the surface EMG. It demonstrates the feasibility of obtaining simultaneous and proportional control signals at multiple DOFs for a prosthesis. The proposed approach is based on a biologically inspired generation model of the surface EMG. The model provides an explicit expression of the surface EMG in terms of *force functions*, which correspond to the intended activations of physiological DOFs of natural movements. When DOF 3 is excluded, the proposed algorithm is capable of capturing nearly 80% of the variance of the forces at 2 DOF.

The most important feature of the proposed DOF-wise NMF algorithm is its semi-unsupervised nature. It does not require recording force signals. The only information regrading the forces required by the algorithm is which DOF is activated in specific contractions during the training contractions. Another advantage of the algorithm is its computational simplicity: only the MSVs of the EMG and simple matrix manipulation is required, making it easy to implement the algorithm in real time.

REFERENCES

[1] B. Hudgins, P. Parker, and R. N. Scott, "A new strategy for multifunction myoelectric control," *IEEE Trans. Biomed. Eng.*, vol. 40, no. 1, pp. 82–94, Jan. 1993.

[2] K. Englehart, B. Hudgins, P. A. Parker, and M. Stevenson, "Classification of the myoelectric signal using time–frequency based representations," *Med. Eng. Phys.*, vol. 21, no. 6/7, pp. 431–438, Jul./Sep. 1999.

[3] A. B. Ajiboye and R. F. Weir, "A heuristic fuzzy logic approach to EMG pattern recognition for multifunctional prosthesis control," *IEEE Trans. Neural Syst. Rehabil. Eng.*, vol. 13, no. 3, pp. 280–291, Sep. 2005.

[4] K. A. Farry, I. D. Walker, and R. G. Baraniuk, "Myoelectric teleoperation of a complex robotic hand," *IEEE Trans. Robot. Autom.*, vol. 12, no. 5, pp. 775–788, Oct. 1996.

[5] N. Jiang, K. B. Englehart, and P. A. Parker, "Extracting neural drives from surface emg: A generative model and simulation studies," in *Proc. IEEE 29th Annu. Int. Conf. Eng. Med. Biol. Soc. 2007*, Aug. 22–26, pp. 4838–4841.

[6] C. S. Sherrington, *The Integrative Action of the Nervous System*. Cambridge, U.K.: Cambridge Univ. Press, 1948.

[7] S. Grillner, "Control of locomotion in bipeds, tetrapods and fish," in *Handbook of Physiology: Sect. 1. The Nervous System*, Bethesda, MD: Amer. Physiol. Soc., 1981, pp. 1179–1236.

[8] F. A. Mussa-Ivaldi, S. F. Giszter, and E. Bizzi, "Linear combinations of primitives in vertebrate motor control," *Proc. Nat. Acad. Sci. USA*, vol. 91, no. 16, pp. 7534–7538, 1994.

[9] P. Saltiel, K. Wyler-Duda, A. d'Avella, M. C. Tresch, and E. Bizzi, "Muscle synergies encoded within the spinal cord: Evidence from focal intraspinal nmda iontophoresis in the frog," *J. Neurophysiol.*, vol. 85, no. 2, pp. 605–619, Feb. 2001.

[10] M. C. Tresch, P. Saltiel, and E. Bizzi, "The construction of movement by the spinal cord," *Nat. Neurosci.*, vol. 2, no. 2, pp. 162–167, Feb. 1999.

[11] E. Bizzi, F. A. Mussa-Ivaldi, and S. Giszter, "Computations underlying the execution of movement: A biological perspective," *Science*, vol. 253, no. 5017, pp. 287–291, 1991.

[12] S. F. Giszter, F. A. Mussa-Ivaldi, and E. Bizzi, "Convergent force fields organized in the frog's spinal cord," *J. Neurosci.*, vol. 13, no. 2, pp. 467–491, 1993.

[13] M. C. Tresch and E. Bizzi, "Responses to spinal microstimulation in the chronically spinalized rat and their relationship to spinal systems activated by low threshold cutaneous stimulation," *Exp. Brain Res.*, vol. 129, no. 3, pp. 401–416, 1999.

[14] F. A. Mussa-Ivaldi, S. F. Giszter, and E. Bizzi, "Linear combinations of primitives in vertebrate motor control," *Proc. Nat. Acad. Sci. USA*, vol. 91, no. 16, pp. 7534–7538, 1994.

[15] F. Gandolfo, F. A. Mussa-Ivaldi, and E. Bizzi, "Motor learning by field approximation," *Proc. Nat. Acad. Sci. USA*, vol. 93, no. 9, pp. 3843–3846, 1996.

[16] L. H. Ting and J. M. Macpherson, "A limited set of muscle synergies for force control during a postural task," *J. Neurophysiol.*, vol. 93, no. 1, pp. 609–613, Jan. 2005.

[17] S. A. Overduin, A. d'Avella, J. Roh, and E. Bizzi, "Modulation of muscle synergy recruitment in primate grasping," *J. Neurosci.*, vol. 28, no. 4, pp. 880–892, 2008.

[18] A. d'Avella, A. Portone, L. Fernandez, and F. Lacquaniti, "Control of fast-reaching movements by muscle synergy combinations," *J. Neurosci.*, vol. 26, no. 30, pp. 7791–7810, Jul. 2006.

[19] C. J. DeLuca, R. S. LeFever, M. P. McCue, and A. P. Xenakis, "Control scheme governing concurrently active human motor units during voluntary contractions," *J. Physiol.*, vol. 329, pp. 129–142, Aug. 1982.

[20] C. J. DeLuca and Z. Erim, "Common drive in motor units of a synergistic muscle pair," *J. Neurophysiol.*, vol. 87, no. 4, pp. 2200–2204, Apr. 2002.

[21] C. J. DeLuca and B. Mambrito, "Voluntary control of motor units in human antagonist muscles: Coactivation and reciprocal activation," *J. Neurophysiol.*, vol. 58, no. 3, pp. 525–542, Sep. 1987.

[22] P. Grosse, M. J. Cassidy, and P. Brown, "EEG–EMG, MEG–EMG and EMG–EMG frequency analysis: Physiological principles and clinical applications," *Clin. Neurophysiol.*, vol. 113, no. 10, pp. 1523–1531, 2002.

[23] D. Winter, *Biomechanics and Motor Control of Human Movement*. New York: Wiley, 1990.

[24] N. Jiang, P. Parker, and K. Englehart, "Spectrum of the nonstationary electromyographic signal modeled with integral pulse frequency modulation and its application to estimating neural drive information," *J. Electromyogr. Kinesiol.*, to be published.

[25] M. C. Tresch, V. C. Cheung, and A. d'Avella, "Matrix factorization algorithms for the identification of muscle synergies: Evaluation on simulated and experimental data sets," *J. Neurophysiol.*, vol. 95, no. 4, pp. 2199–2212, Apr. 2006.

[26] M. Solomonow, R. V. Baratta, B. Zhou, M. Bernardi, and S. Acierno, "Analysis of EMG crosstalk in neighboring and antagonist cat muscles," in *Proc. IEEE 17th Annu. Int. Conf. Eng. Med. Biol. Soc. 1995*, Sep. 20–23, vol. 2, pp. 1353–1354.

[27] C. J. DeLuca and R. Merletti, "Surface myoelectric signal cross-talk among muscles of the leg," *Electroencephalogr. Clin. Neurophysiol.*, vol. 69, no. 6, pp. 568–575, Jun. 1988.

[28] J. W. Morrenhof and H. J. Abbink, "Cross-correlation and cross-talk in surface electromyography," *Electromyogr. Clin. Neurophysiol.*, vol. 25, no. 1, pp. 73–79, Jan./Feb. 1985.

[29] K. Roeleveld, D. F. Stegeman, H. M. Vingerhoets, and A. V. Oosterom, "Motor unit potential contribution to surface electromyography," *Acta Physiol. Scand.*, vol. 160, no. 2, pp. 175–183, Jun. 1997.

[30] D. Farina, C. Févotte, C. Doncarli, and R. Merletti, "Blind separation of linear instantaneous mixtures of nonstationary surface myoelectric signals," *IEEE Trans. Biomed. Eng.*, vol. 51, no. 9, pp. 1555–1567, Sep. 2004.

[31] D. Farina, M. F. Lucas, and C. Doncarli, "Optimized wavelets for blind separation of nonstationary surface myoelectric signals," *IEEE Trans. Biomed. Eng.*, vol. 55, no. 1, pp. 78–86, Jan. 2008.

[32] A. Hyvärinen and P. Pajunen, "Nonlinear independent component analysis: Existence and uniqueness results," *Neural Netw.*, vol. 12, no. 3, pp. 429–439, 1999.

[33] D. D. Lee and H. S. Seung, "Learning the parts of objects by non-negative matrix factorization," *Nature*, vol. 401, no. 6755, pp. 788–791, 1999.

[34] E. J. Bayly, "Spectral analysis of pulse frequency modulation in the nervous systems," *IEEE Trans. Biomed. Eng.*, vol. BME-15, no. 4, pp. 257–265, Oct. 1968.

[35] A. J. Fuglevand, D. A. Winter, and A. E. Patla, "Models of recruitment and rate coding organization in motor-unit pools," *J. Neurophysiol.*, vol. 70, no. 6, pp. 2470–2488, Dec. 1993.

[36] G. V. Dimitrov and N. A. Dimitrova, "Precise and fast calculation of the motor unit potentials detected by a point and rectangular plate electrode," *Med. Eng. Phys.*, vol. 20, pp. 374–381, 1998.

Ning Jiang (S'02) received the B.S. degree in electrical engineering from Xi'an Jiaotong University, Xi'an, China, in 1998, the M.Sc. and Ph.D. degrees in engineering from the University of New Brunswick (UNB), Fredericton, NB, Canada, in 2002 and 2009, respectively.

He is currently a Research Assistant Professor at the Center for Sensory-Motor Interaction, Department of Health Science and Technology, Aalborg University, Aalborg, Denmark. His research interests include signal processing of EMG, EEG, advanced prosthetic control, neuro-rehabilitation, and neuromuscular modeling.

Kevin B. Englehart (S'86–M'99–SM'03) received the B.Sc. degree in electrical engineering and the M.Sc. and Ph.D. degrees from the University of New Brunswick (UNB), Fredericton, NB, Canada, in 1989, 1992, and 1998, respectively.

He is currently a Professor in the Department of Electrical and Computer Engineering, UNB, where he is also the Associate Director of the Institute of Biomedical Engineering. His current research interests include neuromuscular modeling and biological signal processing using adaptive systems, pattern recognition, and time–frequency analysis.

Dr. Englehart is a Registered Professional Engineer, and a member of the IEEE Engineering in Medicine and Biology Society, the IEEE Computer Society, and the Canadian Medical and Biological Engineering Society.

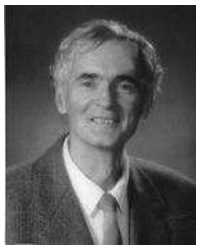

Philip A. Parker (S'70–M'73–SM'86) received the B.Sc. degree in electrical engineering and the Ph.D. degree from the University of New Brunswick (UNB), Fredericton, NB, Canada, in 1964 and 1975, respectively, and the M.Sc. degree from the University of St. Andrews, St. Andrews, U.K., in 1966.

In 1966, he joined the National Research Council of Canada as a Communications Officer. He is currently a Policy Board Member of the Institute of Biomedical Engineering, UNB, which he joined in 1967 as a Research Associate. In 1976, he was appointed to the Department of Electrical Engineering, UNB, where he is currently a Professor Emeritus. His current research interests include the area of biological signal processing with applications to powered limb prosthesis control, evoked response detection/estimation, conduction velocity distribution estimation, and diagnostic tools.